

## The Electron Firehose and Ordinary-Mode Instabilities in Space Plasmas

M. Lazar<sup>1,2</sup> · S. Poedts<sup>1</sup> · R. Schlickeiser<sup>2</sup>  
· D. Ibscher<sup>2</sup>

Received ; accepted

© Springer ●●●

**Abstract** The selfgenerated wave fluctuations are particularly interesting in the solar wind and magnetospheric plasmas, where Coulomb collisions are rare and cannot explain the observed states of quasi-equilibrium. Linear theory predicts that the firehose and the ordinary-mode instabilities can develop under the same conditions, confusing the role of these instabilities in conditioning the space-plasma properties. The hierarchy of these two instabilities is reconsidered here for nonstreaming plasmas with an electron temperature anisotropy  $T_{\parallel} > T_{\perp}$ , where  $\parallel$  and  $\perp$  denote directions with respect to the local mean magnetic field. In addition to the previous comparative analysis, here the entire 3D wave-vector spectrum of the competing instabilities is investigated, paying particular attention to the oblique firehose instability and the relatively poorly known ordinary-mode instability. Results show a dominance of the oblique firehose instability with a threshold lower than the parallel firehose instability and lower than the ordinary-mode instability. For larger anisotropies, the ordinary mode can grow faster, with maximum growth rates exceeding the ones of the oblique firehose instability. In contrast to previous studies that claimed a possible activity of the ordinary-mode in the small  $\beta[< 1]$  regimes, here it is rigorously shown that only the large  $\beta[> 1]$  regimes are susceptible to these instabilities.

**Keywords:** Corona; Flares, Dynamics; Solar wind; Instabilities; Waves, Plasma

### 1. Introduction

Because space-plasmas are hot and weakly collisional, large deviations from thermal equilibrium are expected to be observed even for periods of a quiet Sun. But this is not confirmed by the *in-situ* measurements of the particle velocity distributions, which show a relatively small temperature anisotropy for both

---

<sup>1</sup>Center for Mathematical Plasma Astrophysics, K.U. Leuven, Celestijnenlaan 200B, 3001 Leuven, Belgium

<sup>2</sup>Institut für Theoretische Physik, Lehrstuhl IV: Weltraum- und Astrophysik, Ruhr-Universität Bochum, D-44780 Bochum, Germany, (e-mail: mlazar@tp4.rub.de).

species: electrons and ions (or protons) (for a review, see Marsch, 2006). Kinetic instabilities have been found to be very efficient to reduce the free energy and scatter particles, preventing an increase of the temperature anisotropy, *e.g.* an increase of temperature in the direction of a guiding magnetic field is predicted by the adiabatic expansion (Gary, 1993; Gary *et al.*, 1999; Hellinger *et al.*, 2006; Stverak *et al.*, 2008; Bale *et al.*, 2009).

Here we assume such an excess of parallel temperature, namely,  $T_{\parallel} > T_{\perp}$  (where  $\parallel$  and  $\perp$  denote directions relative to the uniform magnetic field), which can drive two distinct instabilities: the firehose instability (FHI) and the ordinary-mode instability (OMI). The FHI has been extensively studied (see, for instance, Gary, 1993, Li and Habbal, 2000, Gary and Nishimura, 2003, Paesold and Benz, 2003, Camporeale and Burgess, 2008, Lazar and Poedts, 2009 and references therein), providing a quite precise picture of its potential role in temperature isotropization and energy dissipation in the solar wind, flares, and coronal mass ejections. The OMI is less known in this context. This is an aperiodic instability, driven by the velocity anisotropy of plasma particles, *e.g.* streams, temperature anisotropy, in the direction of lower energy. These features suggest a close kinship with the Weibel instability originally described by Weibel (1959) and Fried (1959) in field-free plasmas. In the presence of a uniform magnetic field  $[\mathbf{B}_0]$ , an excess of parallel temperature  $[T_{\parallel} > T_{\perp}]$  may destabilize the ordinary-mode  $[\delta\mathbf{E} \perp \mathbf{B}_0]$  in the perpendicular direction  $\mathbf{k} \perp \mathbf{B}_0$ . Recently, the OMI has been reexamined (Ibscher, Lazar, and Schlickeiser, 2012), providing an accurate characterization of the instability conditions, and these results are invoked in the present analysis.

Recent investigations (Lazar and Poedts, 2009; Lazar, Schlickeiser, and Poedts, 2010) suggest a potential competition between these instabilities at high frequencies, where both the FHI and OMI are driven by electrons with  $T_{e,\parallel} > T_{e,\perp}$ . Thus, for the relaxation of sufficiently large anisotropies, linear dispersion theory predicts maximum growth rates comparable to the proton gyrofrequency for the parallel FHI, while growth rates of the OMI can be several orders of magnitude larger (see Figures 2 and 3). On the other hand, the anisotropy threshold of the FHI seems to be lower, giving to this instability chances to develop, but only for small anisotropies close to the threshold values. However, analytical approximations proposed to describe the OMI solutions in the limit of large wavelengths (larger than the electron gyroradius, *i.e.*  $\lambda \equiv k^{-1} > \rho_e \equiv u_{e,\perp}/\Omega_e$ ; Hamasaki, 1968), may lead to unrealistic estimations of the instability threshold (compare Figure 4 with the results of Lazar, Schlickeiser, and Poedts, 2010). A realistic analysis should also include the oblique FHI  $[0 < \theta < \pi/2]$ , which develops faster than the parallel branch (Paesold and Benz, 1999; Gary and Nishimura, 2003; Camporeale and Burgess, 2008). At oblique angles  $[|\mathbf{k} \cdot \mathbf{B}_0|/(kB_0) = |\cos \theta| \neq 1]$ , this instability exhibits two distinct branches. The first branch is supplied by the propagating modes (with non-zero-frequency  $\omega_r \equiv \Re(\omega) \neq 0$ ), which are also present in the direction parallel to the magnetic field. But the FHI seems to be dominated by the second branch of non-propagating (or zero-frequency  $\omega_r = 0$ ) modes, which occur only for oblique propagation  $[\mathbf{k} \times \mathbf{B}_0 \neq 0]$ .

For a clear picture, we propose to compare the growing modes starting from the orientation of their wave-field vectors in Figure 1. Thus, while the propagating FHI is a shear transverse mode (Figure 1 (a)), the non-propagating FHI (Figure 1 (b)) has a compressive component  $\delta B_{\parallel} = \delta B \sin \theta \neq 0$ , which becomes dominant at large angles of propagation, *i.e.*  $|\delta B_{\parallel}| > |\delta B_{\perp}|$ . The ordinary-mode is linearly polarized, and the orientation of the wave-field vectors is shown in Figure 1 (c). To correlate and extract maximum of information from recent numerical simulations, we keep their settings choosing the coordinate system such that both  $\mathbf{B}_0$  and the wave-vector  $[\mathbf{k}]$  lie in the  $x-z$  plane (Gary and Nishimura, 2003). These simulations clearly demonstrate that i) the fluctuating fields during the growth phase are due to a zero-frequency mode, and ii) throughout the growth, saturation, and subsequent decay of the fields, the dominant component of the fluctuating magnetic field is  $\delta B_y$ , satisfying  $|\delta B_x|^2 \ll |\delta B_z|^2 \ll |\delta B_y|^2$ . According to Figure 1, a major fluctuating magnetic component  $\delta B_y$  cannot be attributed to the non-propagating FHI. It could be associated with the propagating FHI mode, but growth rates of this oscillatory mode are much lower, and it is not confirmed by simulations. Instead, the OMI (Figure 1 (c)) could offer a plausible explanation, as it drives a purely growing (non-propagating) magnetic field fluctuation  $\delta B_y$ . However, it is not yet demonstrated whether this instability can arise and compete or not with the oblique FHIs.

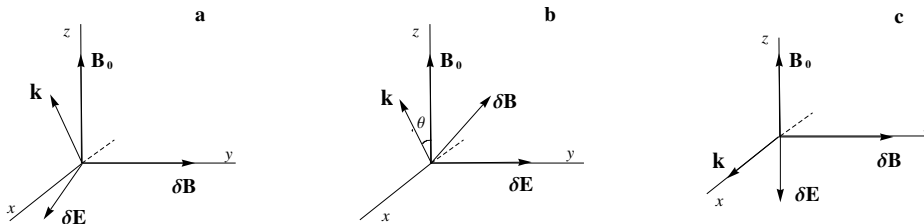


**Figure 1.** The wave electric and magnetic-field orientation: (a) propagating firehose, (b) non-propagating firehose, (c) ordinary-mode (OMI)

The oscillatory (propagating) modes have been extensively investigated to establish their drivers as well as their effects in different scenarios in space plasmas (*e.g.*, see textbook by Gary (1993) and references therein). However, recent studies pay special attention to non-propagating wave instabilities, *e.g.* the compressive mirror and FHIs, and the OMI, which appear to provide better explanations for the observed distributions of data in the solar wind and terrestrial magnetosphere (Hellinger *et al.*, 2006; Stverak *et al.*, 2008; Bale *et al.*, 2009). The *in-situ* measurements of interplanetary magnetic-field fluctuations have indeed confirmed a nearly perpendicular wave-vector [ $k_{\perp} \gg k_{\parallel}$ ] power distribution (Salem *et al.*, 2012). This article is therefore intended to present refined comparative analysis of these instabilities, using recent results for a rigorous characterization of the OMI (Ibscher, Lazar, and Schlickeiser, 2012), and covering the entire 3D wave-vector spectrum of the FHI.

We assume an homogeneous plasma system, largely extended and immersed into an uniform magnetic field  $[\mathbf{B}_0]$ . The unperturbed particle velocity distribution is anisotropic, with an excess of temperature in the direction of the magnetic

field, i.e.,  $T_{\parallel} > T_{\perp}$ . To model this anisotropy, we use a gyrotropic bi-Maxwellian distribution function

$$F_a = \frac{1}{(2\pi)^{3/2} u_{a,\parallel} u_{a,\perp}^2} \exp\left(-\frac{v_{\parallel}^2}{2u_{a,\parallel}^2} - \frac{v_{\perp}^2}{2u_{a,\perp}^2}\right), \quad (1)$$

where  $v_{\parallel}$  and  $v_{\perp}$  are, respectively, the particle velocity components parallel and perpendicular to  $\mathbf{B}_0$ , and  $u_{a,\parallel} = (k_B T_{a,\parallel}/m_a)^{1/2}$  and  $u_{a,\perp} = (k_B T_{\perp,a}/m_a)^{1/2}$  are the corresponding thermal velocities for the plasma particles of types  $a$  ( $a = e$  for electrons,  $a = i$  for ions, and  $a = p$  for protons). The stability analysis of a hot collisionless plasma is based on the linearized Vlasov–Maxwell equations. Here we investigate the unstable wave-mode solutions driven by the anisotropy of the electron temperature, namely, an excess of the parallel temperature, *i.e.*  $T_{e,\parallel} > T_{e,\perp}$ . These modes are the ordinary-mode, which propagates perpendicular to the magnetic field ( $\mathbf{k} \perp \mathbf{B}_0$ ), and the firehose mode, which propagates parallel or obliquely to the magnetic field [ $\mathbf{k} \cdot \mathbf{B}_0 \neq 0$ ]. These are schematically shown in Figure 1. In contrast to parallel propagation, where the electrostatic and electromagnetic modes are decoupled and their theory is relatively simple, at oblique or perpendicular propagation the dispersion relations are complicated, and an accurate characterization of their solutions is possible only numerically.

## 2. The Ordinary-Mode Instability (OMI)

For anisotropic plasmas modeled by the distribution function in Equation (1), ordinary modes are described by the dispersion relation (Ibscher, Lazar, and Schlickeiser, 2012)

$$\frac{\omega^2 - k^2 c^2}{\omega_{p,e}^2} = 1 + \frac{2}{A_e} e^{-\frac{k^2 u_{e,\perp}^2}{\Omega_e^2}} \sum_{n=1}^{\infty} \frac{n^2 \Omega_e^2 I_n(k^2 u_{e,\perp}^2 / \Omega_e^2)}{\omega^2 - n^2 \Omega_e^2}, \quad (2)$$

where  $I_n$  are the modified Bessel functions of the first kind, and  $A = T_{\perp}/T_{\parallel}$  corresponds to the temperature anisotropy. Because the ions (protons) are much heavier than the electrons ( $m_i > m_p \gg m_e$ ), their effects can be neglected at sufficiently high frequencies, and we can assume that they are rigid or isotropically distributed ( $T_{\parallel} = T_{\perp}$ ). The marginal instability threshold can be calculated nu-

**Table 1.** The anisotropy thresholds ( $\gamma_m = 0$ ) from Equation (3) for different values of  $\beta_{e,\parallel}$ .

$\beta_{e,\parallel}$	2.5	5	8	16	30	60	100	500	1000
$(A_e)_{\text{threshold}}$	0.014	0.155	0.276	0.442	0.563	0.660	0.711	0.802	0.823

merically solving the dispersion relation in Equation (2) for a maximum growth rate  $\gamma_m \rightarrow 0$  (Ibscher, Lazar, and Schlickeiser, 2012). Here, for simplicity, we use

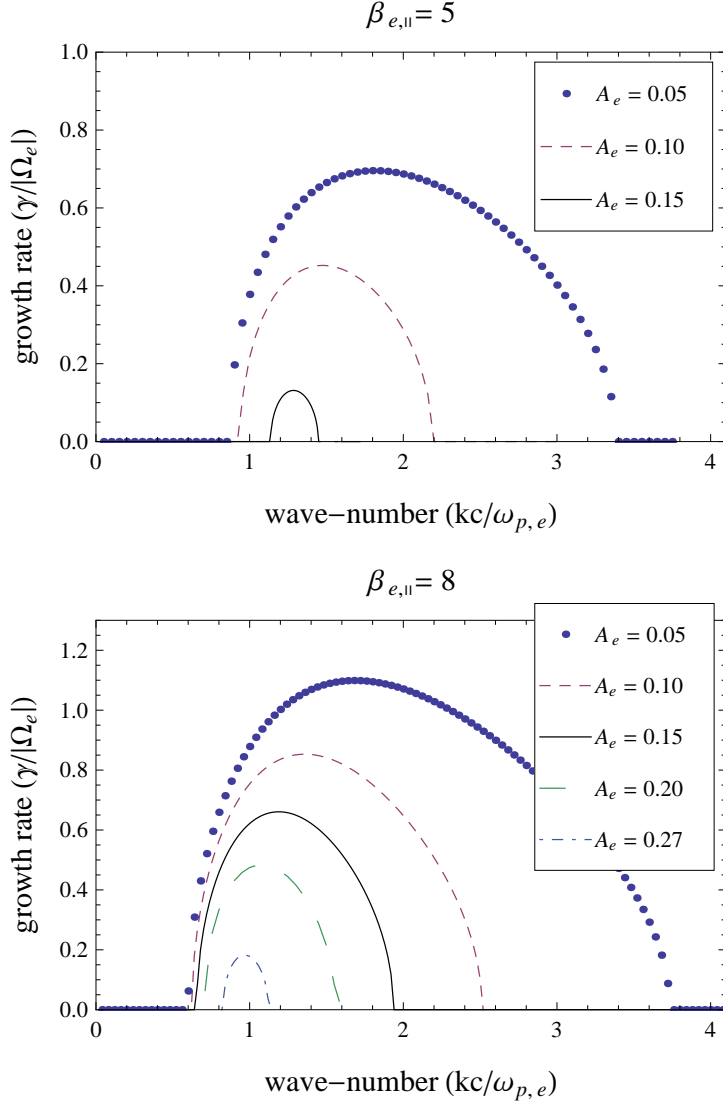


**Figure 2.** Growth rates of the OMI for sufficiently large temperature anisotropies above the threshold (see Table 1):  $A_e < 0.155$  for  $\beta_{e,\parallel} = 5$ , and  $A_e < 0.276$  for  $\beta_{e,\parallel} = 8$ .

the analytical form

$$A_e \leq 1 - \frac{2a(\beta_{e,\parallel})}{\beta_{e,\parallel}}, \quad \text{with} \quad a(\beta_{e,\parallel}) = \ln\left(\frac{w\beta_{e,\parallel}}{2}\right) + \frac{1}{w} I_0\left[\ln\left(\frac{w\beta_{e,\parallel}}{2}\right)\right], \quad (3)$$

which, for a value of the fitting parameter  $w = 0.9$ , provides an accurate fit with the exact numerical threshold (Ibscher, Lazar, and Schlickeiser, 2012). Values

of the anisotropy threshold are given in Table 1 for different values of  $\beta_{e\parallel} \equiv 8\pi n k_B T_{e,\parallel} / B_0^2$ , and are also displayed in Figure 4 (solid line).

Notice that the existence of the OMI is clearly limited to sufficiently large  $\beta_{e,\parallel} [ > 1 ]$  regimes. The exact instability threshold in Equation (3) is markedly different from the instability condition

$$A_e \leq \frac{2}{3} \left( 1 - \frac{1}{\beta_{e,\parallel}} \right)^2, \quad (4)$$

obtained by Hamasaki (1968) in the limit of a small argument of the Bessel function [ $I_n(x < 1)$ ].

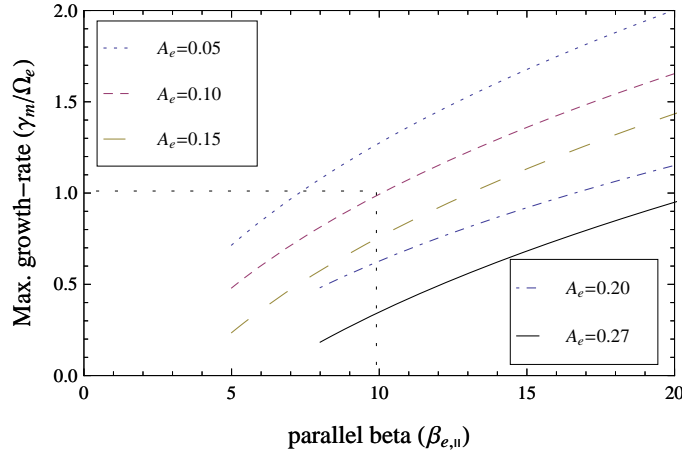


**Figure 3.** Maximum growth rate of the ordinary-mode instability as a function of  $\beta_{e,\parallel}$  for different values of the temperature anisotropy:  $A_e = 0.05, 0.10, 0.15, 0.20$  and  $0.27$ .

Growth rates [ $\gamma = \omega_i$ ] of the OMI are displayed in Figure 3. These are calculated numerically for conditions typically encountered at different altitudes [ $0.3 - 1$  AU] in the solar wind. At the saturation, maximum growth rates [ $\gamma_m$ ] depend only on the plasma beta [ $\beta_{e,\parallel}$ ] and the temperature anisotropy [ $A_e$ ]. For sufficiently large anisotropies,  $\gamma_m$  can approach or exceed  $|\Omega_e|$ , see the right panel in Figure 3. Recent estimates have restricted (Ibscher, Lazar, and Schlickeiser, 2012)

$$\gamma_m \leq \left| k^2 c^2 + \frac{\omega_{p,e}^2}{A_e} \{ A_e - 1 + I_0(g) \exp[-g] \} \right|^{1/2}, \quad (5)$$

where

$$g = \frac{k^2 u_{e,\perp}^2}{\Omega_e^2} = \frac{k^2 c^2 A_e \beta_{e,\parallel}}{\omega_{p,e}^2 2}, \quad (6)$$

but this limit is function of the wavenumber value, and cannot provide general constraints depending only on the plasma parameters. Here, in Figure 3, we derive numerically the exact values of the maximum growth rates [ $\gamma_m$ ] function

of  $\beta_{e,\parallel}$ , and for different values of the temperature anisotropy [ $A_e < 1$ ]. The OMI is enhanced by the temperature anisotropy [ $T_{e,\parallel} > T_{e,\perp}$ ], but it is inhibited by the stationary magnetic field ( $\beta_{e,\parallel} \sim B_0^{-2}$ ).

### 3. Interplay with the Oblique FHI

Previous studies have shown that the parallel FHI cannot compete with the OMI, which is much faster (Lazar and Poedts, 2009; Lazar, Schlickeiser, and Poedts, 2010). Here we give particular attention to the oblique FHI, which grows much faster than the parallel FHI. The predictions of the dispersion theory and numerical confirmations are clear in this case: the parallel firehose instability admits maximum growth rates close to, but less than,  $\Omega_p$  (Gary and Madland, 1985), whereas the oblique firehose instability can reach maximum growth rates two or three orders of magnitudes larger, *e.g.*  $\Omega_p \ll \gamma_m < |\Omega_e|$  (Li and Habbal, 2000; Gary and Nishimura, 2003; Camporeale and Burgess, 2008). Moreover, the anisotropy threshold of the oblique firehose instability is also lower (Paesold and Benz, 1999; Hellinger *et al.*, 2006; Stverak *et al.*, 2008).

At oblique propagation, the electron-firehose instability splits into two different branches, and both develop much faster than the parallel firehose instability. The first branch is the continuation of the parallel firehose instability and is supplied by the propagating (nonzero-frequency) modes. In the second branch, the instability is purely growing (or aperiodic), and is usually called the non-propagating FHI. Now, it is worth mentioning that a powerful numerical resolution of the Vlasov–Maxwell dispersion relations clearly shows that i) the existence of propagating modes at large angles ( $\theta$  up to  $70^\circ - 80^\circ$ ) (even for a small anisotropy  $T_{e,\parallel}/T_{e,\perp} \gtrsim 2$ ); ii) the maximum growth rates are reached for large angles ( $\theta > 45^\circ$ ); and iii) the nonpropagating FHI is largely dominant at these inclinations (Camporeale and Burgess, 2008).

Looking to the field properties in Figure 1, we can add further distinctions between these two branches. Like its proton-driven counterpart, the propagating electron firehose mode (Figure 1 (a)) is a shear (torsional) transverse wave that twists magnetic field lines relative to one another but does not compress (Swanson, 2003; Gary and Nishimura, 2003). This mode is nonresonant with electrons but resonant with ions (Gary, 1993; Paesold and Benz, 1999), enabling the transfer of energy from electrons to protons, and thus supporting the transit-time damping scenario. On the other hand, the nonpropagating [ $\omega_r = 0$ ] mode (Figure 1 (b)) has a compressive component,  $\delta B_{\parallel} \neq 0$ , parallel to the mean magnetic field. When this is small, that is, when  $|\delta B_{\parallel}| < |\delta B_{\perp}|$  [small angles  $\theta$ ], the instability is predominantly transverse and cyclotron resonant with electrons, and it can therefore play an important role in the relaxation of their anisotropy (Gary and Nishimura, 2003). When the parallel component is large, that is when  $|\delta B_{\parallel}| > |\delta B_{\perp}|$ , the instability is predominantly compressive, like the electron mirror instability, which also has  $\omega_r = 0$ , but is driven by an opposite anisotropy  $T_{e,\perp} > T_{e,\parallel}$  (Pokhotelov *et al.*, 2002; Gary and Karimabadi, 2006). Notice that the thresholds of these two instabilities provide the best fit to the observed limits of the temperature anisotropy in space plasmas (Hellinger *et al.*, 2006; Stverak

*et al.*, 2008). In this case, the wave magnetic field not only rotates but changes its magnitude as well. Landau damping of this nonpropagating mode can be very efficient at scattering electrons in phase space (Gary and Karimabadi, 2006).

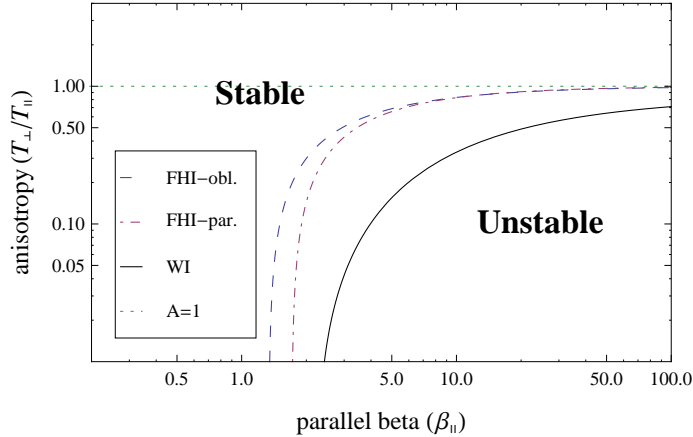


**Figure 4.** The instability thresholds: comparison of the parallel FHI (dash-dotted line), the non-propagating FHI (long-dashed line) and the OMI (solid line).

In Figure 4, we compare the anisotropy thresholds of these two instabilities. The propagating FHI corresponds to the dash-dotted line, and the non-propagating FHI corresponds to the dashed line. The exact thresholds are derived numerically for finite, but very small values of the growth rate, e.g.,  $\gamma_m = 10^{-2}\Omega_p$ , close to the marginal condition of stability [ $\gamma_m = 0$ ]. The isolines of constant growth rate derived from linear theory are usually fitted with

$$\frac{T_{e,\perp}}{T_{e,\parallel}} = 1 - \frac{S}{\beta_{e,\parallel}^\alpha}. \quad (7)$$

Values of the fitting parameters [ $S$  and  $\alpha$ ] derived for a  $\gamma_m = 10^{-2}\Omega_p$  are shown in Table 2 (after Gary and Nishimura, 2003).

**Table 2.** Values of the fitting parameters  $S$  and  $\alpha$  in Equation (7).

$(\gamma_m = 10^{-2}\Omega_p)$	Propagating FHI	Nonpropagating FHI
$S$	1.70	1.29
$\alpha$	0.99	0.88

For comparison, the threshold of the OMI as given by Equation (3) is illustrated in Figure 4 with the solid line. We can also fit to power laws of the form in Equation (7), but Equation (3) is the best analytical description of the instability threshold (see the analysis by Ibscher, Lazar, and Schlickeiser, 2012). Thresholds



of the FHI are lower than those of the OMI, but the maximum growth rates of the latter increase much faster with  $\beta_{e,\parallel}$  (*e.g.* see Figure 3), leading to values larger than  $|\Omega_e|$ , which is the limit derived numerically for the nonpropagating FHI (Gary and Nishimura, 2003; Camporeale and Burgess, 2008). This supports our result that for sufficiently large anisotropies, *e.g.*  $T_{e,\parallel}/T_{e,\perp} > 10$ , or sufficiently large  $\beta_{e,\parallel} > 10$ , the OMI is faster than the FHI and can manifest itself as the principal mechanism of relaxation. Larger values of  $\beta_{e,\parallel}$  means less intense magnetic fields [ $B_0$ ], or/and more dense and hotter plasma populations, so that these conditions can be encountered at different altitudes in the solar wind.

#### 4. Discussion and Conclusions

We have used results of the linear Vlasov-Maxwell theory to compare the properties of two growing modes driven by  $T_{e,\parallel} > T_{e,\perp}$ : the FHI and the OMI. In addition to previous analyses, here the entire 3D wave-vector spectrum of the competing instabilities is examined, paying particular attention to the non-propagating FHI. Before drawing the main conclusions of our article, we examine the conditions for the initiation of these instabilities in recent numerical simulations, and in solar-wind observations. Numerical studies have reported on linear and quasi-linear developments of the electron FHI in PIC simulations (Messmer, 2002; Gary and Nishimura, 2003; Camporeale and Burgess, 2008) and test particle simulations (Paesold and Benz, 2003). The conditions implemented in these experiments are typical for the solar wind, or for the impulsive solar flares. To shed more light on these results, we refer again to the wave-field vectors representation in Figure 1. We keep the settings from the simulations choosing the coordinate system such that both  $\mathbf{B}_0$  and the wave-vector  $[\mathbf{k}]$  lie in the  $x-z$  plane (Gary and Nishimura, 2003; Camporeale and Burgess, 2008).

Numerical simulations demonstrated that i) the fluctuating fields during the growth phase are due to a nonpropagating (zero-frequency) mode, and ii) throughout the growth phase, the saturation phase, and the subsequent decay phase of the fields, the dominant component of the fluctuating magnetic field is  $|\delta\mathbf{B}| = \delta B_y$ , satisfying  $|\delta B_x|^2 \ll |\delta B_z|^2 \ll |\delta B_y|^2$ . (In the article by Camporeale and Burgess (2008), the cartesian system is rotated, such that the dominant component is  $\delta B_z$ , but this corresponds to the same component perpendicular to both  $\mathbf{k}$  and  $\mathbf{B}_0$ .) This component has been attributed to the nonpropagating FHI, which can extend to quasi-perpendicular directions and grows faster than the propagating FHI. However, the orientation of the wave-field vectors in Figure 1 demonstrates that a major fluctuating magnetic component  $\delta B_y$  cannot be attributed to the non-propagating FHI. Moreover, at large, quasi-perpendicular angles  $[\theta]$ , the nonpropagating mode is highly compressional and exhibits large parallel fluctuations  $\delta B_{\parallel} = \delta B_z$ . Instead, magnetic-field fluctuations along the  $y$ -axis direction, perpendicular to  $\mathbf{B}_0$ , can be driven by the propagating FHI, but this is time-oscillatory (nonzero-frequency) and less apparent in the early stage of the simulation. The OMI is also a plausible candidate as it is a zero-frequency mode of comparable wavelength (*i.e.*  $\approx c/\omega_{p,e}$ , that is the electron skin-depth, see Figure 2 above and Figure 3 of Camporeale and Burgess (2008)).

Now we apply the results of this article to check if the OMI is fast enough to develop and to compete with the FHI under the same conditions of the two sets of PIC simulations (Gary and Nishimura, 2003; Camporeale and Burgess, 2008). If we consider the representative run F-257 from the 1D PIC simulations of Gary and Nishimura (2003), with initial parameters  $\beta_{e,\parallel} = 7.7$  and  $A_e = T_{e,\perp}/T_{e,\parallel} = 0.46$ , the OMI cannot set in, because the instability threshold in Equation (3) requires a temperature anisotropy  $A_e < 0.27$ . The same result is obtained if we check all the other 1D runs (F-250, F-252, and F-255), or the 2D runs of Camporeale and Burgess (2008), concluding that none of these PIC simulations are relevant for the OMI. The instability cannot be initiated when  $A_e$  is above the threshold.

Large temperature anisotropies [ $T_{e,\parallel} \gg T_{e,\perp}$ ] are believed to arise in flares and other violent phenomena in the solar wind, such as the co-rotating forward and reversed shocks in coronal mass ejections. Under these conditions, the parallel  $\beta$  can cover a wide interval of values ( $0.01 < \beta_{e,\parallel} < 100$ ), and the OMI is much easier excited, offering plausible explanations for the observed emissions and suprathermal populations. For instance, for a moderate value of  $\beta_{e,\parallel} = 8$ , the instability threshold in Equation (3) requires a temperature anisotropy  $A_e < 0.28$ . This is equivalent with a minimum  $T_{e,\parallel}/T_{e,\perp} > 3.6$  that is well below the large temperature anisotropies [ $T_{e,\parallel}/T_{e,\perp} > 10$ ] predicted by the observations in flares. Such scenarios have been implemented in numerical simulations, but only the parallel FHI has been examined (Messmer, 2002; Paesold and Benz, 2003), without indications from directions perpendicular to the magnetic field. More information can be extracted from the solar-wind observations of their proton-driven counterparts. Measurements of the magnetic-field fluctuations show an enhanced magnetic compressibility along the mirror instability threshold (at  $T_{\perp} > T_{\parallel}$  and large  $\beta_{\parallel} > 1$ ), but small elsewhere (Bale *et al.*, 2009). This is consistent with our results, which suggest non-compressive instability constraints for the opposite anisotropies  $T_{\perp} < T_{\parallel}$ . However, the magnetic compressibility is increasing with increasing  $\beta_{\parallel}$  (Figure 1 of Bale *et al.* (2009)), reaching values comparable with the mirror instability if  $\beta_{\parallel} > 8$  is large enough, and indicating traces of the quasi-perpendicular compressive modes.

**Table 3.** Properties of the wave instabilities driven by  $T_{\parallel} > T_{\perp}$ .

Instability	Growth rate	Threshold	Propagation	Fluctuating fields
OMI, $\omega_r = 0$	$\gamma_m >  \Omega_e $	High	$\theta = \pi/2$	$\delta\mathbf{E} \parallel \mathbf{B}_0$
FHI, $\omega_r \neq 0$	$\gamma_m \ll  \Omega_e $	Low	$0 \leq \theta < \pi/2$	$\delta\mathbf{B} \perp \mathbf{B}_0$
FHI, $\omega_r = 0$	$\gamma_m <  \Omega_e $	Lower	$0 < \theta < \pi/2$	$\delta\mathbf{B}_{\parallel} \neq 0$

In conclusion, the comparative analysis of the wave instabilities driven in a magnetized plasma by an excess of parallel temperature predicts a dominance of the non-propagating FHI with a threshold lower than that of the parallel FHI and lower than that of the OMI. However, for larger anisotropies, the ordinary mode can develop faster with maximum growth rates exceeding that of the non-propagating FHI. The properties of the competing wave instabilities have

been summarized in Table 3. In contrast to previous studies that claimed a possible activity of the OMI in the small  $\beta < 1$  regimes, here it is rigorously shown that only the large  $\beta > 1$  regimes are susceptible to these instabilities. The existing numerical simulations are dedicated to the FHI, and cannot offer information about the OMI because the settings are far below the threshold condition. Numerical simulations confirm the predictions of the dispersion theory that the fastest growing mode is aperiodic. However, according to our analysis, the dominant component of the fluctuating magnetic field indicated by the simulations (perpendicular to  $\mathbf{B}_0$ ) cannot be attributed to the non-propagating FHI, but to the OMI, or, eventually, to the propagating FHI, although such a time-oscillatory mode is not reported in the early linear stage of the simulations. Motivated by these results, the next numerical investigations should consider supplementary conditions for the OMI to develop, and examine the interplay with the FHI in both stages of linear growth and nonlinear saturation.

**Acknowledgements** ML acknowledges financial support from the EU Commission and Research Foundation Flanders (FWO) as FWO Pegasus Marie Curie Fellow (grant 1.2.070.13). The authors acknowledge support from the Ruhr-Universität Bochum, the Deutsche Forschungsgemeinschaft (DFG), grant Schl 201/21-1, and by the Katholieke Universiteit Leuven. These results were obtained in the framework of the projects GOA/2009-009 (KU Leuven), G.0729.11 (FWO-Vlaanderen) and C 90347 (ESA Prodex 9). The research leading to these results has also received funding from the European Commission's Seventh Framework Programme (FP7/2007-2013) under the grant agreements SOLSPANET (project n 269299, www.solspanet.eu), SPACECAST (project n 262468, fp7-spacecast.eu), eHeroes (project n 284461, www.eheroes.eu) and SWIFF (project n 263340, www.swiff.eu).

## References

- Bale, S., Kasper, J.C., Howes, G.G., Quataert, E., Salem, E., Sundkvist, D.: 2009, Magnetic fluctuation power near proton temperature anisotropy instability thresholds in the solar wind. *Phys. Rev. Lett.* **103**, 211101. doi:10.1103/PhysRevLett.103.211101.
- Camporeale, E., Burgess, D.: 2008, Electron firehose instability: Kinetic linear theory and two-dimensional particle-in-cell simulations. *J. Geophys. Res.* **113**, A07107. doi:10.1029/2008JA013043.
- Fried, B.D.: 1959, Mechanism for instability of transverse plasma waves. *Phys. Fluids* **2**, 337. doi:10.1063/1.1705933.
- Gary, S.P.: 1993, *Theory of Space Plasma Microinstabilities*, University Press, Cambridge.
- Gary, S.P., Karimabadi, H.: 2006, Linear theory of electron temperature anisotropy instabilities: Whistler, mirror, and Weibel. *J. Geophys. Res.* **111**, A11224. doi:10.1029/2006JA011764.
- Gary, S.P., Madland, D.: 1985, Electromagnetic electron temperature anisotropy instabilities. *J. Geophys. Res.* **90**, 7607-7610. doi:10.1029/JA090iA08p07607.
- Gary, S.P., Neagu, E., Skoug, R.M., Goldstein, B. E.: 1999, Solar wind electrons: Parametric constraints. *J. Geophys. Res.* **104**, 19843-19849. doi:10.1029/1999JA900244.
- Gary, S.P., Nishimura, K.: 2003, Resonant electron firehose instability: Particle-in-cell simulations. *Phys. Plasmas* **10**, 3571-3576. doi:10.1063/1.1590982.
- Hamasaki, S.: 1968, Electromagnetic microinstabilities of plasmas in a uniform magnetic induction. *Phys. Fluids* **11**, 2724-2727. doi:10.1063/1.1691879.
- Hellinger, P., Travnicek, P., Kasper J.C., Lazarus, A.J.: 2006, Solar wind proton temperature anisotropy: Linear theory and WIND/SWE observations. *Geophys. Res. Lett.* **33**, L09101. doi:10.1029/2006GL025925.
- Ibscher, D., Lazar, M., Schlickeiser, R.: 2012, On the existence of Weibel instability in a magnetized plasma. II. Perpendicular wave propagation: The ordinary mode. *Phys. Plasmas* **19**, 072116. doi:10.1063/1.4736992.

- Lazar, M., Poedts, S.: 2009, Limits for the firehose instability in space plasmas. *Solar Phys.* **258**, 119-128. doi:10.1007/s11207-009-9405-y.
- Lazar, M., Schlickeiser, R., Poedts, S.: 2010, Nonresonant electromagnetic instabilities in space plasmas: interplay of Weibel and firehose instabilities. In: *AIP Conf. Proc.* **1216**, 280-283. doi:10.1063/1.3395855.
- Li, X., Habbal, S.R.: 2000, Electron kinetic firehose instability. *J. Geophys. Res.* **105**, 27377-27385. doi:10.1029/2000JA000063.
- Marsch, E.: 2006, Kinetic physics of the solar corona and solar wind. *Living Rev. Solar Phys.* **3**, 1. doi:10.12942/lrsp-2006-1.
- Messmer, P.: 2002, Temperature isotropization in solar flare plasmas due to the electron firehose instability. *Astron. Astrophys.* **382**, 301-311. doi:10.1051/0004-6361:20011583.
- Paesold, G., Benz, A.O.: 1999, Electron firehose instability and acceleration of electrons in solar flares. *Astron. Astrophys.* **351**, 741-746.
- Paesold, G., Benz, A.O.: 2003, Test particle simulation of the electron firehose instability. *Astron. Astrophys.* **401**, 711-720. doi:10.1051/0004-6361:20030113.
- Pokhotelov, O.A., Treumann, R.A., Sagdeev, R.Z., Balikhin, M.A., Onishchenko, O.G., Pavlenko, V.P., Sandberg, I.: 2002, Linear theory of the mirror instability in non-Maxwellian space plasmas. *J. Geophys. Res.* **107**, 1312. doi:10.1029/2001JA009125.
- Salem, C.S., Howes, G.G., Sundkvist, D., Bale, S.D., Chaston, C.C., Chen, C.H.K., Mozer, F.S.: 2012, Identification of kinetic Alfvén wave turbulence in the solar wind. *Astrophys. J.* **745**, L9. doi:10.1088/2041-8205/745/1/L9.
- Schlickeiser, R., Lazar, M., Skoda, T.: 2011, Spontaneously growing, weakly propagating, transverse fluctuations in anisotropic magnetized thermal plasmas. *Phys. Plasmas* **18**, 012103. doi:10.1063/1.3532787.
- Stverak, S., Travnicek, P., Maksimovic, M., Marsch, E., Fazakerley, A.N., Scime, E.E.: 2008, Electron temperature anisotropy constraints in the solar wind. *J. Geophys. Res.* **113**, A03103. doi:10.1029/2007JA012733.
- Swanson, D.G.: 2003, *Plasma Waves, 2nd Edition*, IOP Publishing Ltd., Bristol and Philadelphia.
- Weibel, E.S.: 1959, Spontaneously growing transverse waves in a plasma due to an anisotropic velocity distribution. *Phys. Rev. Lett.* **2**, 83-84. doi:10.1103/PhysRevLett.2.83.

This figure "f1a.png" is available in "png" format from:

<http://arxiv.org/ps/1307.0768v1>

This figure "f1b.png" is available in "png" format from:

<http://arxiv.org/ps/1307.0768v1>

This figure "f1c.png" is available in "png" format from:

<http://arxiv.org/ps/1307.0768v1>

This figure "f2a.png" is available in "png" format from:

<http://arxiv.org/ps/1307.0768v1>



This figure "f2b.png" is available in "png" format from:

<http://arxiv.org/ps/1307.0768v1>

This figure "f3.png" is available in "png" format from:

<http://arxiv.org/ps/1307.0768v1>

This figure "f4.png" is available in "png" format from:

<http://arxiv.org/ps/1307.0768v1>